Proceedings of the 2005 IEEE
International Conference on Robotics and Automation
Barcelona, Spain, April 2005

Automatic Guidance of a Surgical Instrument with Ultrasound Based Visual Servoing

Marie-Aude Vitrani, Guillaume Morel, and Tobias Ortmaier
Laboratoire de Robotique de Paris (LRP)
University of Paris 6, CNRS (FRE2507), Paris, France
{*vitrani, morel, ortmaier*}*@robot.jussieu.fr*

***Abstract*— Visual servoing is a possible solution to assist the surgeon in performing tasks under ultrasound (US) imaging. To this aim, a system was developed that allows the surgeon to select a desired instrument location on a US image. Then a robot is programmed to automatically move the instrument towards the selected location. This approach requires robust tracking of the instrument in the US image, together with modeling of the overall system and implementation of a visual servoing loop. This paper presents geometrical and kinematic models of the system, as well as the control loop design, which is validated through both numerical simulations, and results of in vitro experiments.**

***Index Terms*— Image-guided surgery, visual servoing, ultrasound.**

I. Introduction

The ultrasound (US) imaging techniques were introduced in medicine in the 1950s. These low cost devices provide high resolution images in real time. They are used mostly for pure imaging purposes (that is in the sole aim of producing images), but also in a few intervention procedures. In this case, the surgeon moves an instrument inside a patient while observing the motion of the instrument with an outer ultrasound probe. This requires high coordination skills. Indeed, the ultrasound image gives only a 2D cross-section of the 3D working volume which contains no depth information. Therefore, manual US guided interventions are mainly limited to simple tasks such as puncture [1].

In order to ease the manipulation under ultrasound observation, a possible solution is to automatically realize the hand/eye synchronization. The proposed approach consists in an image guided robotic system using US-based visual servoing: in the US image the instrument is detected and a desired position is specified by the surgeon. The position error is then used in a visual servoing loop to move the instrument towards the specified goal. This loop guarantees that the surgical instrument is always visible in the US image.

In the literature, only little research is reported on the use of an ultrasound probe in a robotic system. The proposed systems can be divided into two groups.

In the first group, a robot is used to manipulate an ultrasound probe. In most of these papers, the US image is considered as an output of the system, but it is not used as a measurement device to control the robot motion. Here, the robot allows for remote US imaging (*e.g.* [2], [3]), or for enhanced quality imaging, thanks to the control of the force applied by the probe to the patient [4]. In contrast, in [5], a telemanipulated probe holder is presented with automatic visual tracking features. Its control is shared between the surgeon and a visual servoing loop. This loop is aimed at automatically tracking features extracted from a region of interest which corresponds to a given anatomic structure (*e.g.* a carotid artery). This system allows for enhanced imaging capabilities, such as physiological motion compensation, since the probe holder moves in order to obtain a fixed image of the tracked target.

In the second group of papers, which correspond to the scope of our research, a robot is used to move an instrument under the supervision of a US imaging system. In [6], a computer-assisted robotic system is used for ultrasound-guided biopsy. A robot holds a needle, which is to be inserted into an organ under the supervision of the surgeon. The system provides the surgeon with a reconstructed 3D view of the probe and the needle, but there is no automatic guidance feature. Furthermore, the 3D reconstruction requires a number of additional equipments to localize the US probe and the needle. In [7], a robotic system is presented, which includes a manipulator moving a surgical instrument towards a target. Automatic tracking of the target is provided, and fed to the robot controller. However, this system can be viewed as *indirect* visual servoing: the visual servo loop is not expressed in the image. Rather, the robot position is controlled from a 3D measurement obtained by image tracking. As a result, the system requires additional equipment to measure the position of the probe with respect to the manipulator, together with extensive calibration procedures to estimate the geometric transforms between several equipments. This prevents for an application to a clinical case, since in vitro experimental results exhibit positioning errors as large as 15 mm (in terms of standard deviation errors). Finally, in [8], *direct* visual servoing is used to automatically guide a needle for a percutaneous cholecystostomy. A mechatronic device is presented, comprising a US probe and a 2 degrees of freedom needle manipulator. The needle is mechanically constrained to lie within the US plane. Its orientation and penetration are automatically controlled thanks to a visual servoing loop aimed at placing the needle tip into a tracked target. This stronlgy limits the application to a particular kind of planar tasks.

In this paper, we consider the broader problem of controlling an instrument that does not entirely lie in the US plane. The

0-7803-8914-X/05/$20.00 ©2005 IEEE.

proposed approach is based on direct visual servoing of the points corresponding to the intersection of the instrument with the ultrasound plane. A conventional, model based, approach of the visual servoing controller design is used [9]. In contrast to most of the cited papers, the approach proposed in this paper does not require any cumbersome additional localizer. Indeed, only a rough estimate of the probe location with respect to the robot is needed in order to evaluate the so-called *image jacobian*, that maps the instrument velocity into the image features velocity.

The rest of paper is organized as follows: the next section introduces the surgical task and describes the complete system. Then, the geometrical and kinematic models are derived in Sect. III. In Sect. IV the control loop is presented. Sect. V gives experimental results. The last section concludes this paper.

II. System description

A. Notations

In the subsequent sections, the following notations are used:
a for a scalar,
A for a point,
${}^C\mathbf{a}$ for a vector which coordinates are expressed in the base $\mathcal{B}_C$ of the frame $\mathcal{F}_C$ attached to the point C,
$\mathbf{A}$ for a matrix,
$\mathbf{d}_{AB}$ is the vector from point A to point B,
$\left[{}^C\mathbf{a}\right]_\times$, the skew symmetric matrix associated with ${}^C\mathbf{a}$, so that for any vector ${}^C\mathbf{b}$, $\left[{}^C\mathbf{a}\right]_\times {}^C\mathbf{b} = {}^C\mathbf{a} \times {}^C\mathbf{b}$.

B. System Description

The considered task is a minimally invasive heart mitral valve repair operation. Our research, in cooperation with partners of the Gabie/Robea CNRS program, focuses on the following scenario for the intervention:

1) a US probe is placed in the oesophagus of the patient;
2) a small incision is made in the patient torso, and a trocar is placed in order to allow for an access into the left ventricle;
3) an instrument (a pair of forceps), held by a robot manipulator, is carefully introduced in the trocar;
4) the surgeon rotates the US probe plane until he/she locates the instrument;
5) a visual servoing loop is then lauchned, aimed at automatically control the position of the instrument in the US image. This provides two kinds of capabilities:
   - if the desired image location stays still, while the surgeon moves the probe, then the instrument automatically follows the probe motion in order to keep a constant image position;
   - if the probe stays still, and the surgeon indicates in the screen a new desired location, then the instrument automatically moves towards the desired location while staying in the image plane.

The overall system is sketched in Fig. 1. In this figure, one can observe that the system is designed so that the intersection of the surgical tool with the US plane is represented by two points (in fact, *blobs*) in the image.

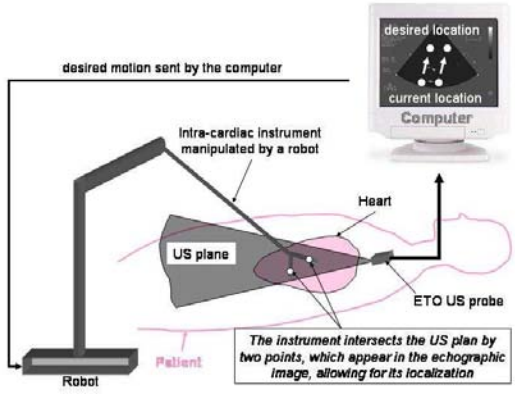

Fig. 1. System Description

III. Modeling

The following assumptions are made in order to model the system:

- The geometrical and kinematic models of the robot are considered to be well-known.
- The US image is assumed to be a 2D cross-section of the 3D workspace (referred as *echographic plane* or *echographic image*).
- The US probe pose (i.e. position and orientation) with respect to the robot base is assumed to be known (the robustness with respect to errors in this model will be studied in Sect. IV).

A. Geometrical Model

The instrument $\mathcal{I}$ is modeled with three straight lines intersecting at point I: one line represents the instrument axis, the other two lines model the jaws of the forceps. The intersection of the US plane Π with the forceps is modeled by two points denoted M_1 and M_2, see Fig. 2(a).

Three orthonormal coordinate frames are defi ned, Fig. 2(a):

- $\mathcal{F}_T = \{T;\ {}^T\mathbf{i}_T,\ {}^T\mathbf{j}_T,\ {}^T\mathbf{k}_T\}$ is the coordinate frame attached to the robot base at point T which denotes the trocar,
- $\mathcal{F}_P = \{P;\ {}^P\mathbf{i}_P,\ {}^P\mathbf{j}_P,\ {}^P\mathbf{k}_P\}$ is the coordinate frame attached to the US probe with ${}^P\mathbf{k}_P$ is perpendicular to the US plane, and P the origin of the US rays,
- $\mathcal{F}_I = \{I;\ {}^I\mathbf{i}_I,\ {}^I\mathbf{j}_I,\ {}^I\mathbf{k}_I\}$ is the coordinate frame attached to the instrument. The vector ${}^I\mathbf{k}_I$ is parallel to the instrument axis, Fig. 2(b).

The matrix $\mathbf{R}_{\mathcal{I}\to\mathcal{P}}$ represents the rotation from the instrument frame to the US frame. $\mathbf{d}_{TI} = -d\mathbf{k}_I$ and $\mathbf{d}_{IM_i} = l_i\mathbf{t}_i$ for $i = \{1, 2\}$. Furthermore, ${}^I\mathbf{t}_1 = [-t_x\ 0\ -t_z]^T$ and ${}^I\mathbf{t}_2 = [t_x\ 0\ -t_z]^T$ with $t_x^2 + t_z^2 = 1$.

The geometrical model expresses the instrument coordinates $\mathbf{s} = [x_{M_1}, y_{M_1}, x_{M_2}, y_{M_2}]^T$ in the US image as a function of instrument pose.

As M_1 and M_2 belong both to the instrument and to the US

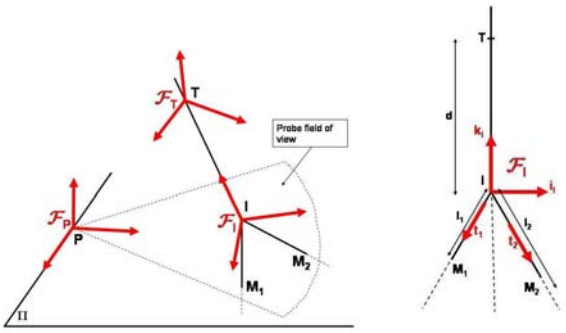

(a) Frames (b) Tool model

Fig. 2. Geometrical parameters

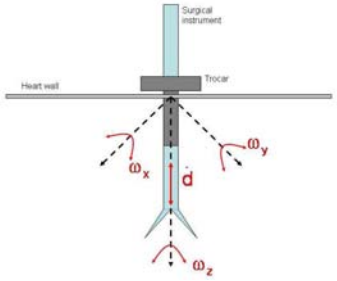

Fig. 3. Degrees of freedom used when manipulating through a trocar

plane, the geometrical model must verify:

$$\begin{cases} l_i \mathbf{t}_i \;=\; \mathbf{d}_{IM_i} \;, \\ \\ ({}^P\mathbf{k}_P)^T \; {}^P\mathbf{d}_{PM_i} \;=\; 0 \;. \end{cases} \qquad i = \{1,2\} \tag{1}$$

Thus, the model can be expressed in the base $\mathcal{B}_P$ as:

$${}^P\mathbf{s} \;=\; \begin{bmatrix} 1 & 0 & -\frac{{}^P t_{1x}}{{}^P t_{1z}} \\ 0 & 1 & -\frac{{}^P t_{1y}}{{}^P t_{1z}} \\ 1 & 0 & -\frac{{}^P t_{2x}}{{}^P t_{2z}} \\ 0 & 1 & -\frac{{}^P t_{2y}}{{}^P t_{2z}} \end{bmatrix} {}^P\mathbf{p} \;. \tag{2}$$

where

$$\begin{aligned} \mathbf{p} \;&=\; [x_I, y_I, z_I]^T \;, \\ {}^P\mathbf{t}_i \;&=\; \mathbf{R}_{\mathcal{I}\to\mathcal{P}} \, {}^I\mathbf{t}_i \;. \end{aligned}$$

B. Image Jacobian

In the intervention scenario, the instrument is introduced into the heart through a trocar fixed on the heart wall, see Fig. 3. Hence, only four intracardiac degrees of freedom remain. Three of these remaining kinematic variables are the elements of ${}^I\mathbf{\Omega}_{\mathcal{I}/\mathcal{P}} = [\omega_x,\ \omega_y,\ \omega_z]^T$, the angular velocity of the instrument tip with respect to the US probe. The last kinematic variable is $\dot{d}$, the translational velocity of the instrument tip along the instrument axis.

In order to control these four degrees of freedom, four independent variables characterizing the instrument displacement in the US image were chosen: the desired 2D velocity of the points M_1 and M_2 in the US plane.

Therefore, the kinematic model is the relation giving the velocity of the points M_1 and M_2 in the echographic plane as a function of the kinematic variables ${}^I\mathbf{\Omega}_{\mathcal{I}/\mathcal{P}}$ and $\dot{d}$:

$$\dot{\mathbf{s}} = \mathbf{J} \left[\omega_x \;\omega_y \;\omega_z \;\dot{d}\right]^T \;. \tag{3}$$

where $\mathbf{J}$ is the *so-called* image jacobian. In the next, the kinematic relation is derived for one point M_i, then the image jacobian is computed writing the obtained relation for both points M_1 and M_2.

Noticing that M_i is defined as the intersection of the jaw i with a plane, it is not a physical point. Therefore, its velocity with respect to the probe frame, $\mathbf{v}_{M_i/\mathcal{P}}$ writes

$$\mathbf{v}_{M_i/\mathcal{P}} \;=\; \mathbf{v}_{M_i/\mathcal{I}} \;+\; \mathbf{v}_{M_i\in\mathcal{I}/\mathcal{P}} \;, \tag{4}$$

where $\mathbf{v}_{M_i/\mathcal{I}} = \dot{l}_i \mathbf{t}_i$ is the velocity of M_i with respect to the instrument, and $\mathbf{v}_{M_i\in\mathcal{I}/\mathcal{P}}$ is the velocity of the physical point coinciding with M_i at the considered instant, with respect to the probe frame.

Projecting (4) onto the vector $\mathbf{k}_P$ perpendicular to the US plane yields

$$0 = \dot{l}_i \mathbf{k}_P^T \mathbf{t}_i + \mathbf{k}_P^T \mathbf{v}_{M_i\in\mathcal{I}/\mathcal{P}} \tag{5}$$

Using the resulting expression of $\dot{l}_i$ in (4) yields

$$\mathbf{v}_{M_i/\mathcal{P}} \;=\; -\frac{1}{\mathbf{k}_P^T \mathbf{t}_i} \left[\mathbf{k}_P^T \mathbf{v}_{M_i\in\mathcal{I}/\mathcal{P}} \mathbf{t}_i - \mathbf{k}_P^T \mathbf{t}_i \mathbf{v}_{M_i\in\mathcal{I}/\mathcal{P}}\right] \;. \tag{6}$$

Thus, the velocity of the point M_i is:

$$\mathbf{v}_{M_i/\mathcal{P}} \;=\; -\frac{1}{\mathbf{k}_P^T \mathbf{t}_i} \mathbf{k}_P \times \left(\mathbf{t}_i \times \mathbf{v}_{M_i\in\mathcal{I}/\mathcal{P}}\right) \;. \tag{7}$$

Furthermore, as T is an invariant point, one has (using similar notations as for (4)):

$$\mathbf{v}_{T/\mathcal{P}} = 0 = \underbrace{\mathbf{v}_{T/\mathcal{P}}}_{\dot{d}\mathbf{k}_I} + \mathbf{v}_{T\in\mathcal{I}/\mathcal{P}} \;. \tag{8}$$

Thus, the velocity of the physical point coinciding with M_i is:

$$\mathbf{v}_{M_i\in\mathcal{I}/\mathcal{P}} \;=\; -\dot{d}\,\mathbf{k}_I \;+\; (d\,\mathbf{k}_I \;-\; l_i \mathbf{t}_i) \times \mathbf{\Omega}_{\mathcal{I}/\mathcal{P}} \;. \tag{9}$$

The relation giving the velocity of M_i in the US plane as a function of the kinematic variables is obtained when substituting ${}^I\mathbf{v}_{M_i\in\mathcal{I}/\mathcal{P}}$ from (9) into (7):

$$\begin{aligned} \mathbf{v}_{M_i/\mathcal{P}} \;=\; & -\frac{1}{\mathbf{k}_P^T \mathbf{t}_i} \mathbf{k}_P \times \\ & \left[\mathbf{t}_i \times \left(-\dot{d}\mathbf{k}_I \;+\; (d\mathbf{k}_I - l_i \mathbf{t}_i) \times \mathbf{\Omega}_{\mathcal{I}/\mathcal{P}}\right)\right] \end{aligned} \tag{10}$$

This relation, expressed in the base $\mathcal{B}_P$, can be rewritten into the following matrix equation:

$$\begin{bmatrix} {}^P v_{(M_i/\mathcal{P})x} \\ {}^P v_{(M_i/\mathcal{P})y} \end{bmatrix} \;=\; \mathbf{J}_{M_i} \begin{bmatrix} \omega_x \\ \omega_y \\ \omega_z \\ \dot{d} \end{bmatrix} \;=\; \mathbf{J}_{M_i}\, \mathbf{u} \;, \tag{11}$$

$$\dot{\mathbf{s}} \;=\; \mathbf{J}\,\mathbf{u} \;=\; \left[\begin{array}{c}\mathbf{J}_{M_1}\\ \mathbf{J}_{M_2}\end{array}\right]\mathbf{u}\;. \tag{12}$$

The jacobian matrix can be written as:

$$\mathbf{J} \;=\; \mathbf{S}\,\mathbf{R}^T\,\mathbf{A}\,\mathbf{B} \tag{13}$$

where:

$$\mathbf{S}=\left[\begin{array}{cccccc}1&0&0&0&0&0\\0&1&0&0&0&0\\0&0&0&1&0&0\\0&0&0&0&1&0\end{array}\right],\;\mathbf{R}=\left[\begin{array}{cc}\mathbf{R}_{\mathcal{I}\rightarrow\mathcal{P}}&\mathbf{0}_{3\times3}\\\mathbf{0}_{3\times3}&\mathbf{R}_{\mathcal{I}\rightarrow\mathcal{P}}\end{array}\right],$$

$$\mathbf{A}=\left[\begin{array}{cc}\frac{-\left[{}^I\mathbf{k}_P\right]_\times}{\mathbf{k}_P^T\,\mathbf{t}_1}&\mathbf{0}_{3\times3}\\\mathbf{0}_{3\times3}&\frac{-\left[{}^I\mathbf{k}_P\right]_\times}{\mathbf{k}_P^T\,\mathbf{t}_2}\end{array}\right],$$

$$\mathbf{B}=\left[\begin{array}{cc}-l_1\left[{}^I\mathbf{t}_1\right]_\times^2&\left[{}^I\mathbf{t}_1\right]_\times\\-l_2\left[{}^I\mathbf{t}_2\right]_\times^2&\left[{}^I\mathbf{t}_2\right]_\times\end{array}\right]\left[\begin{array}{cccc}1&0&0&0\\0&1&0&0\\0&0&1&0\\0&-d&0&0\\d&0&0&0\\0&0&0&-1\end{array}\right].$$

C. Inverse Jacobian

To solve the inverse kinematics problem, the four kinematic variables must be computed from the 2D velocity of M_1 and M_2. This can be done by inverting (7), which can be rewritten as :

$$\mathbf{k}_P\times\left(\mathbf{t}_i\times\mathbf{v}_{M_i\in\,\mathcal{I}/\mathcal{P}}\right) \;=\; -\left(\mathbf{k}_P^T\,\mathbf{t}_i\right)\,\mathbf{v}_{M_i/\mathcal{P}}\;. \tag{14}$$

In order to solve this equation for $\mathbf{v}_{M_i\in\,\mathcal{I}/\mathcal{P}}$, the following theorems are applied:

$$\left\{\begin{array}{l}\forall\, r,(\mathbf{a}\times\mathbf{x}=\mathbf{b})\Leftrightarrow\left(\mathbf{x}=r\,\mathbf{a}-\frac{1}{\mathbf{a}^2}\mathbf{a}\times\mathbf{b}\text{ if }\mathbf{a}^T\mathbf{b}=0\right)\;,\\ \forall\,\mathbf{x},\;\;(\mathbf{a}\times\mathbf{x})^T\;\mathbf{a}\;=\;0\;.\end{array}\right. \tag{15}$$

The obtained solution is:

$$\begin{aligned}\mathbf{v}_{M_i\in\,I/\mathcal{P}} &= r_i\,\mathbf{t}_i+\mathbf{t}_i\times\left[\mathbf{t}_i\times\left(\mathbf{k}_P\times\left(\mathbf{k}_P\times\mathbf{v}_{M_i/\mathcal{P}}\right)\right)\right]\\ &= r_i\,\mathbf{t}_i\;-\;\mathbf{t}_i\times\left(\mathbf{t}_i\times\mathbf{v}_{M_i/\mathcal{P}}\right)\end{aligned} \tag{16}$$

for all r_i being an arbitrary scalar.
Substituting $\mathbf{v}_{M_i\in\,I/\mathcal{P}}$ from (9) into (16), the relation between the kinematic variables and $\mathbf{v}_{M_i/\mathcal{P}}$ is:

$$\begin{aligned}\forall\; r_i,\;\; -\dot{d}\mathbf{k}_I-(d\mathbf{k}_I+l_i\mathbf{t}_i)\times\mathbf{\Omega}_{I/\mathcal{P}} =\\ r_i\,\mathbf{t}_i-\mathbf{t}_i\times\left(\mathbf{t}_i\times\mathbf{v}_{M_i/\mathcal{P}}\right)\;.\end{aligned} \tag{17}$$

To derive the inverse kinematic model this equation is projected onto the vectors $\mathbf{k}_I$, $\mathbf{j}_I$ and $\mathbf{t}_i$ for each point M_i. Thus, a six equations system with six unknowns (r_1, r_2, and the kinematic variables: ω_x, ω_y, ω_z, and $\dot{d}$) is obtained. Thereafter, the kinematic variables are expressed as functions of the 2D velocity of M_1 and M_2 by solving the previous system. Then, the inverse kinematic model can be written in a matrix form:

$$\mathbf{u} \;=\; \mathbf{J}^{-1}\,\dot{\mathbf{s}}\;. \tag{18}$$

The inverse image jacobian $\mathbf{J}^{-1}$ is:

$$\mathbf{J}^{-1} \;=\; \mathbf{C}\,\mathbf{R}\,\mathbf{S}^T\;, \tag{19}$$

where $\mathbf{S}$ and $\mathbf{R}$ are the matrix defined in (13), and:

$$\mathbf{C}^T=\left[\begin{array}{cccc}0&\frac{-t_z}{\Delta_2}&0&\frac{t_z(dt_z+l_2)}{t_x\Delta_2}\\\frac{l_2}{\Delta_1}&0&\frac{-(d+l_2t_z)}{t_x\Delta_1}&0\\0&\frac{t_x}{\Delta_2}&0&\frac{-(dt_z+l_2)}{\Delta_2}\\0&\frac{-t_z}{\Delta_2}&0&\frac{-t_z(dt_z+l_1)}{t_x\Delta_2}\\\frac{l_1}{\Delta_1}&0&\frac{(d+l_1t_z)}{t_x\Delta_1}&0\\0&\frac{-t_x}{\Delta_2}&0&\frac{-(dt_z+l_1)}{\Delta_2}\end{array}\right],$$

$$\Delta_1=(l_1+l_2)d+2l_1l_2t_z\;,$$

$$\Delta_2=(l_1+l_2)+2dt_z\;.$$

Note that the obtained inverse jacobian matrix, that can be used in the control loop, depends on two kinds of parameters:

- parameters that rely on the robot and instrument geometry only, and can be supposed to be perfectly known, such as t_x, t_z and d;
- parameters that depend on the location of the probe with respect to the robot, such as $\mathbf{R}_{\mathcal{I}\rightarrow\mathcal{P}}$, l_1 and l_2. In a practical intervention, these can be known only approximately, which may challenge the system robustness.

IV. Control

This section describes the chosen control loop and gives some simulation results. The desired position $\mathbf{s}_d$ is the vector of the desired 2D coordinates of M_1 and M_2 in the US plane. This desired position is specified by the surgeon in the echographic image. The error $\boldsymbol{\varepsilon}$ between the desired and the measured position in the US plane is fed into the controller. The visual servoing loop computes the command velocity vector $\mathbf{u}$ using the inverse kinematic model.
In the control loop, the inverse image jacobian has to be estimated as the jacobian depends on several parameters that are not perfectly known. As the robot kinematics and the instrument geometry are accurately known, the major parameter uncertainties lie in the estimation of the relative pose between US probe and robot base (namely $\mathbf{R}_{\mathcal{I}\rightarrow\mathcal{P}}$, l_1 and l_2). Therefore, only an approximate inverse jacobian matrix $\widehat{\mathbf{J}^{-1}}$ can be used in the controller:

$$\mathbf{u} \;=\; \lambda\,\widehat{\mathbf{J}^{-1}}\,\boldsymbol{\varepsilon} \;=\; \lambda\,\widehat{\mathbf{J}^{-1}}\;(\mathbf{s}_d-\mathbf{s})\;, \tag{20}$$

where λ is a scalar proportional gain. Using the previous control law, the closed-loop behavior of the system is:

$$\dot{\boldsymbol{\varepsilon}}=-\dot{\mathbf{s}}=-\mathbf{J}\mathbf{u}=-\lambda\,\mathbf{J}\,\widehat{\mathbf{J}^{-1}}\boldsymbol{\varepsilon}\;. \tag{21}$$

If all the parameters are perfectly known, the estimated inverse jacobian is equal to the inverse jacobian. Thus, the system closed-loop behavior becomes:

$$\dot{\boldsymbol{\varepsilon}}=-\lambda\,\mathbf{J}\,\mathbf{J}^{-1}\boldsymbol{\varepsilon}=-\lambda\,\boldsymbol{\varepsilon}\;. \tag{22}$$

This equation is linear for $\boldsymbol{\varepsilon}$, which means that the variables are well decoupled. Thus, the error exponentially converges towards zero.
Numerical simulations were performed to evaluate the closed loop behavior of the system. Results for simulation of a perfectly known case are shown in Fig. 4. The error exponentially

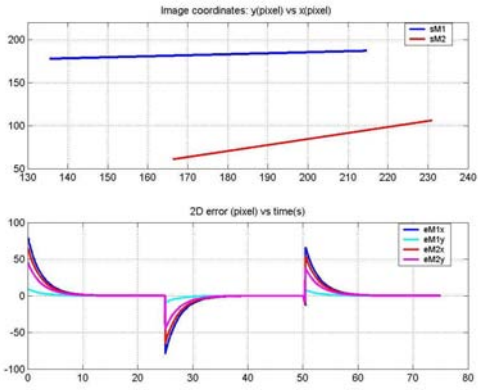

Fig. 4. Simulation result with no estimation error

converges toward zero and the instrument displacement is in straight lines, according to (22).

When parametric uncertainties occur, the analytical expressions of $\mathbf{J}$ and $\widehat{\mathbf{J}^{-1}}$ do not allow to easily perform theoretical studies on the stability of (21). A first observation is that any translation of the US probe parallel to the US plane does not affect the parameters $\mathbf{R}_{\mathcal{I}\to\mathcal{P}}$, l_1 and l_2. Therefore, the jacobian estimation is robust with respect to the positioning uncertainties of the probe along the US plane. The only parameters modifying the inverse image jacobian are the orientation of the US probe with respect to the robot base and the distance between the robot base and the US plane measured along $\mathbf{k}_P$.

In order to pratically study the influence of these errors, extended simulations were performed while including significant amount of errors in the estimation of the location of the probe with respect to the robot base. Simulation results indicate that even within large uncertainties the error still converges toward zero and the control loop is still stable. As an illustration, Fig. 5 displays the closed loop behavior for two kinds of uncertainties:

- errors in the orientation of the probe around the axes $\mathbf{i}_P$, $\mathbf{j}_P$ and $\mathbf{k}_P$,
- translation errors along $\mathbf{k}_P$.

In spite of quite large errors, the system is still stable.

V. Experimental result

A. Set-up

The experimental set-up consists of a box full of water in which an US probe is placed and a surgical tool moved by a robot. The robot (MC2E, french acronym for compact manipulator for endoscopic surgery, developed at the Laboratoire de Robotique de Paris) used to manipulate the instrument is especially suited for minimally invasive robotic surgery applications and provides, with its spherical structure, 4 degrees of freedom at the instrument tip, Fig. 6(a). A force control have been developped on this robot and tested during in vivo experiments. The geometrical and kinematics models of the robot are presented in [10].

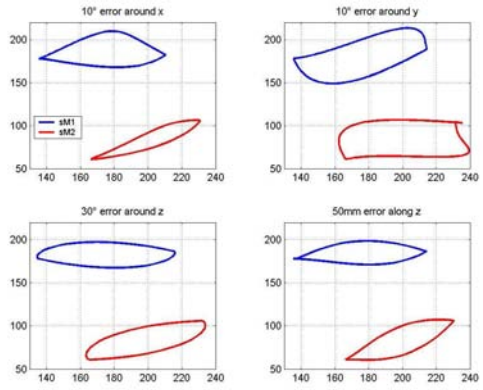

(a) Image coordinates: y(pixel) vs x(pixel)

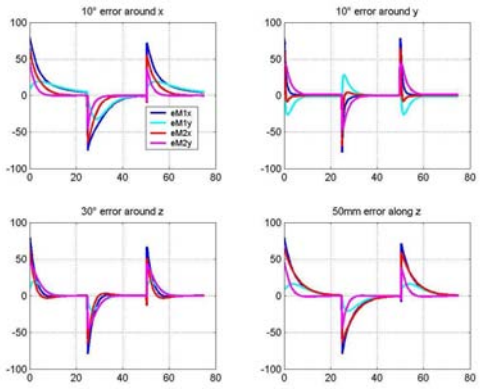

(b) 2D error (pixel) vs time (s)

Fig. 5. Simulation robustness results

To identify the instrument echoes in the echographic image, real time detection, labeling, and tracking algorithms were developed, [11].

As US images are very noisy and contains a lot of artifacts (Fig. 6(b)), the tracking of the instrument must be very robust. The used algorithms compute the coordinate vector $\mathbf{s}$ in pixels. They are converted into metric coordinates using a simple gain that was experimentally identified (0.0008 mm = 1 pixel). The overall computation time is less than 10 ms, thus being bellow the 40 ms frame rate of the US probe.

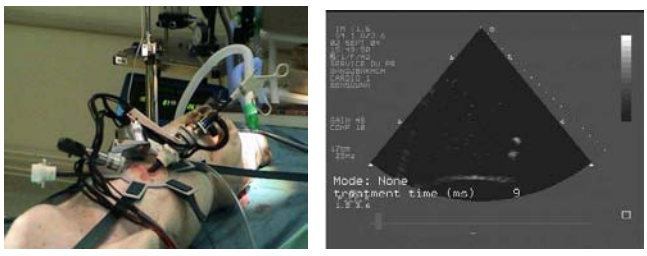

(a) MC2E robot (b) US image

Fig. 6. Elements of the experimental system

B. Results

During experiments, the probe is manually kept under water and its relative pose with respect to the robot base is roughly estimated. The first experiment is performed in order to test the proposed control loop. Two desired instrument positions in the image are selected. The instrument is then moved by visual servoing from one to the other. Figure 7 shows the displacement in the image and the error ε between the desired position and the measured position. As the error exponentially converges toward zero, the closed loop behavior presented in (21) is verified and the variables are well decoupled. This can be seen as well in the coordinates plot where the instrument displacements approximately follow straight lines. The settling time is approximately 6s, which is consistent with the tuned gain $\lambda = 0.4s^{-1}$.

Additional experiments were performed in order to test the

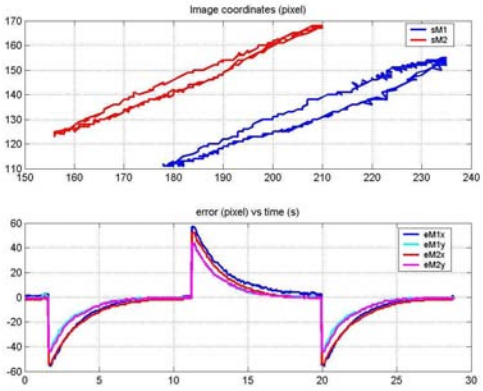

Fig. 7. Experiment results with no estimation error

control loop robustness. Namely, the experiment as previously described was run including an error in the estimation of the probe orientation around $\mathbf{k}_P$. The results are shown in Fig. 8, for an increasing orientation error. Similarly to the simulation results, the control loop shows good robustness in the conducted experiments: although the exponential convergence is not guaranteed anymore, the system finally converges towards its desired value. Note that, due to the integral effect in the loop, the final error is always zero, up to the measurement noise, which was experimentally found to be less than +/- 1 pixel. This correspond to a geometric positioning error of less than 1 mm.

VI. Conclusion

A robotic system with US imaging has been presented in this paper. It uses US based visual servoing to control the position of an instrument inside the heart. The experimentally observed robustness during in vitro validation is encouraging in the perspective of in vivo experiments.

Acknowledgment

The financial support of the CNRS P.I.R. Robea program is gratefully ackowledged. The authors also warmly thank Dr. Mourad Karouia, and M.D. Nicolas Bonnet (Cardiac Surgery Service of the Pitié Salpêtrière Hospital, Paris, France) for their help during the experiments.

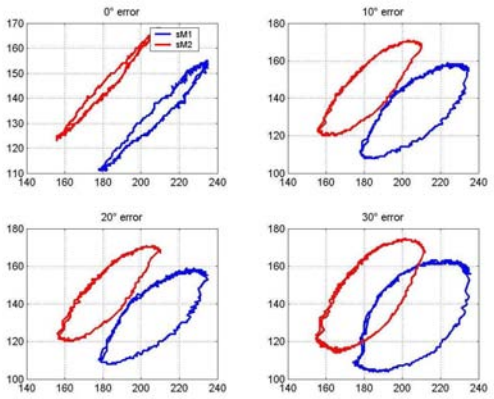

Fig. 8. Experiments robustness results

References

[1] L. Angelini and M. Caratozzolo. Intraoperative echography: the state of the art. *Ann. Ital. Chir*, 70(2):223–230, March-April 1999.

[2] A. Gourdon, P. Poignet, G. Poisson, Y. Parmantier, and P. Marche. Master slave robotic system for ultrasound scanning. In *IEEE Medical and Biological Engineering Conference, Proceedings*, Vienna, Austria, November 1999.

[3] A. Vilchis, J. Troccaz, P. Cinquin, A. Guerraz, F. Pellisier, P. Thorel, B. Tondu, F. Courrges, G. Poisson, M. Althuser, and J. Ayoubi. Experiments with the ter tele-echography robot. In *Medical Image Computing and Computer-Assisted Intervention - MICCAI 2002: 5th International Conference, Proceedings, Part I*, pages 138 – 146, Tokyo, Japan, September 25-28 2002.

[4] F. Pierrot, E. Dombre, E. Dégoulange, L. Urbain, P. Caron, S. Boudet, J. Gariépy, and J.L. Mégnien. Hippocrate: a safe robot arm for medical applications with force feedback. *Medical Image Analysis*, 3(3):285–300, 1999.

[5] S.E. Salcudean, W.H. Zhu, P. Abolmaesumi, S. Bachmann, and P.D. Lawrence. A robot system for medical ultrasound. *Robotics Research*, May 2000.

[6] G. Megali, O. Tonet, C. Stefanini, M. Boccadoro, V. Papaspyropoulos, L. Angelini, and P. Dario. A computer-assisted robotic ultrasound-guided biopsy system for video-assisted surgery. In *Medical Image Computing and Computer-Assisted Intervention - MICCAI 2001: 4th International Conference, Proceedings*, pages 343–350, Utrecht, The Netherlands, October 2001.

[7] J. Stoll, P. Dupont, and R. Howe. Ultrasound-based servoing of manipulators for telesurgery. In *Telemanipulator and Telepresence Technologies VIII Conference*, volume 4570 of *Proceedings of SPIE*, October 2001.

[8] J. Hong, T. Dohi, M. Hashizume, K. Konishi, and N. Hata. An ultrasound-driven needle insertion robot for percutaneous cholecystostomy. *Physics in Medicine and Biology*, 49(3):441–455, february 2004.

[9] S. Hutchinson, G. Hager, and P. Corke. A Tutorial on Visual Servo Ccontrol. *IEEE Trans. on Robotics and Automation*, 12(5):651–670, 1996.

[10] N. Zemiti, T. Ortmaier, M.-A. Vitrani, and G. Morel. A force controlled laparoscopic surgical robot without distal force sensing. In *Proc. of the ISER 2004; 9th International Symposium on Experimental Robotics*, Singapore, June 2004.

[11] T. Ortmaier, M.-A. Vitrani, G. Morel, and S. Pinault. Robust instrument tracking in ultrasound images for visual servoing. In *Proc. of IEEE ICRA'05: International Conference on Robotics and Automation*, Barcelona, Spain, April 2005.